Stem Cell Reports
Report
OPEN ACCESS

Chemical Conversion of Human Fibroblasts into Functional Schwann Cells

Eva C. Thoma,[1,*] Claudia Merkl,[1,3] Tobias Heckel,[1] Rachel Haab,[1] Frederic Knoflach,[1] Corinne Nowaczyk,[1] Nicholas Flint,[1] Ravi Jagasia,[1] Sannah Jensen Zoffmann,[1] Hoa Hue Truong,[1] Pascal Petitjean,[1] Sebastian Jessberger,[2] Martin Graf,[1] and Roberto Iacone[1]

[1]Roche Pharma Research and Early Development, Roche Innovation Center Basel, 4070 Basel, Switzerland
[2]Brain Research Institute, Faculty of Medicine and Science, University of Zurich, 8057 Zurich, Switzerland
[3]Present address: Novartis Pharma AG, Novartis Institutes for BioMedical Research, Musculoskeletal Diseases, 4056 Basel, Switzerland
*Correspondence: eva_christina.thoma@roche.com
http://dx.doi.org/10.1016/j.stemcr.2014.07.014

SUMMARY

Direct transdifferentiation of somatic cells is a promising approach to obtain patient-specific cells for numerous applications. However, conversion across germ-layer borders often requires ectopic gene expression with unpredictable side effects. Here, we present a gene-free approach that allows efficient conversion of human fibroblasts via a transient progenitor stage into Schwann cells, the major glial cell type of peripheral nerves. Using a multikinase inhibitor, we transdifferentiated fibroblasts into transient neural precursors that were subsequently further differentiated into Schwann cells. The resulting induced Schwann cells (iSCs) expressed numerous Schwann cell-specific proteins and displayed neurosupportive and myelination capacity in vitro. Thus, we established a strategy to obtain mature Schwann cells from human postnatal fibroblasts under chemically defined conditions without the introduction of ectopic genes.

INTRODUCTION

In recent years, the idea of directly converting one somatic cell type into another has attracted substantial attention because it offers a valuable source for cells that are difficult to access (Vierbuchen and Wernig, 2011). However, a major drawback linked to current strategies is the fact that they are based on ectopic expression of key developmental genes that often have to be stably integrated into the genome. Despite the possibilities to tightly control ectopic gene expression, such genetic modifications may have undesired effects. Small molecules specifically modifying key signaling pathways provide a powerful tool to enhance conversion or even replace reprogramming genes. Recently, the generation of pluripotent stem cells in mouse by small molecules has been reported (Hou et al., 2013). However, chemical conversion of human cells has thus far only been demonstrated for the generation of endodermal cells (Pennarossa et al., 2013).

Here, we aimed to convert human fibroblasts into Schwann cells, the major glial cell type of the peripheral nervous system.

Using a multikinase inhibitor, we attempted to convert fibroblasts first into a transient precursor stage showing features of neural crest, the origin of Schwann cells. These transient precursors were then further differentiated into mature Schwann cells. Importantly, the complete cell conversion process did not require the expression of ectopic genes but was solely based on chemical treatment. It thus represents a promising approach to generate patient-specific Schwann cells and proves that cellular identities can be significantly altered by small molecule treatment.

RESULTS

Identification of a Compound Allowing Neural Transdifferentiation

Current protocols for converting one cell type into another often suffer from low efficiencies (Table S1 available online). This might be partially due to the fact that many protocols attempt to obtain postmitotic cell types, e.g., neurons. Thus, the conversion procedure includes a stop of proliferation, which reduces both yield and efficiency. To maximize these parameters, we established a two-step protocol for fibroblast transdifferentiation. First, fibroblasts are converted into a transient, proliferative neural precursor stage. In a second step, these precursors are differentiated into induced Schwann cells (iSCs).

In vivo, Schwann cells arise from the neural crest (NC), a multipotent, neuroepithelial cell population that is specified by numerous signaling cues (Stuhlmiller and García-Castro, 2012). We reasoned that the combination of neural inductive cues together with NC specifiers might induce a NC fate in fibroblasts. As potent neural inducing signal we used a small molecule—compound B (CB)—that had been identified in a high-throughput screen to selectively promote proliferation of neural stem cells while inhibiting their differentiation (Figures 1A–1C). Induction of a proliferative precursor stage in fibroblasts was analyzed by the capacity of sphere formation, an assay widely used to identify cells with progenitor features (Dontu et al., 2003; Tropepe et al., 2000). CB treatment resulted in a significant increase in both sphere size and total cell number (Figure 1D) compared to control-treated cells. Kinase profiling identified CB as potent multikinase inhibitor with the

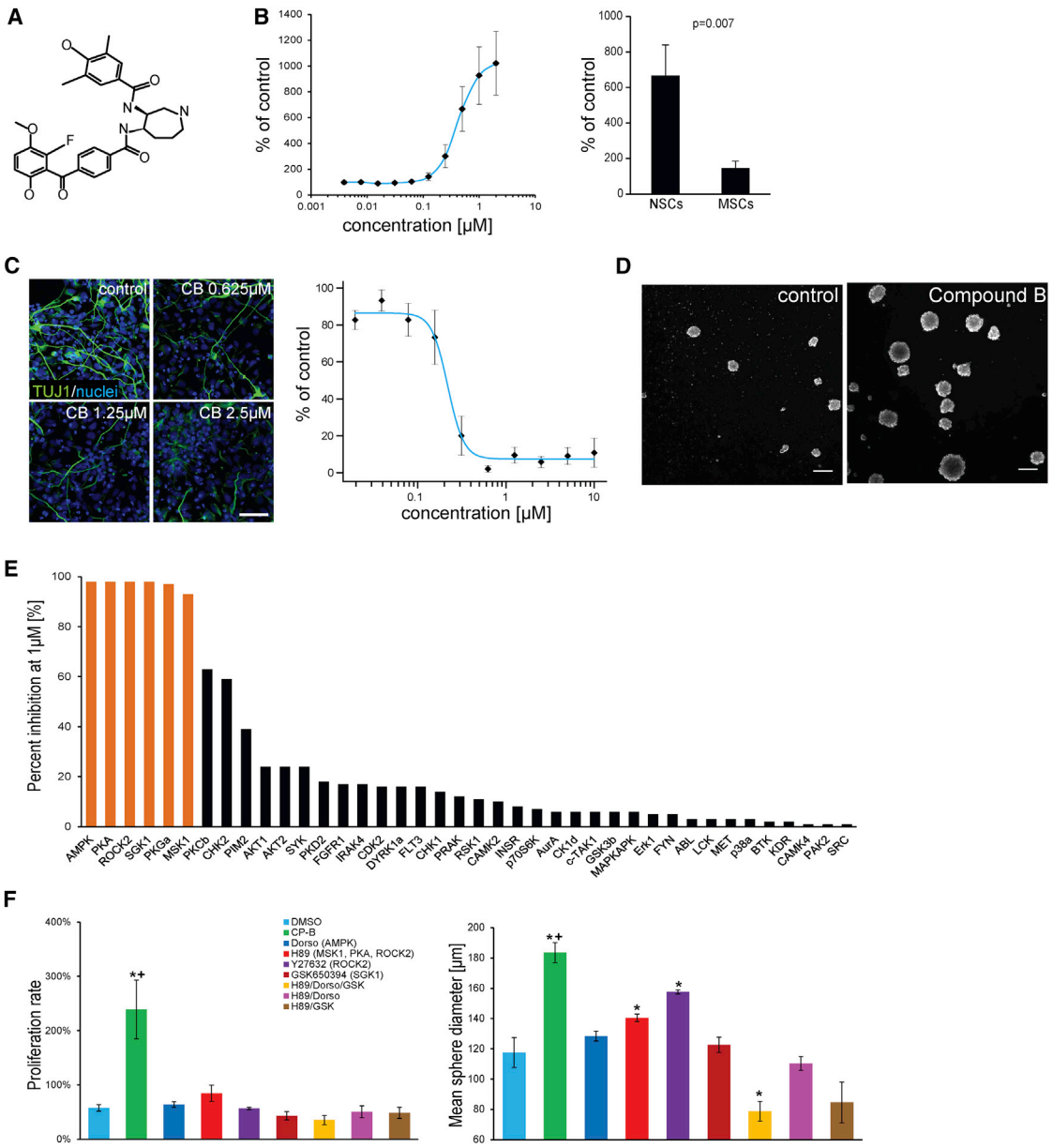

Figure 1. Identification of a Small Molecule Enhancing Neural Stem Cell Proliferation and Enabling Conversion of Fibroblasts into Neurosphere-like Structures

(A) Structure of compound B (CB).

(B) CB selectively promotes proliferation of ESC-NSCs. Proliferation was analyzed by ATP assay. Fold increase to control-treated cells is shown. Left: dose-response assay with ESC-NSCs (n = 4). Right: effect of CB (0.5 μM) on proliferation of ESC-NSCs (n = 4) and ESC-MSCs (n = 2).

(C) CB inhibits differentiation of ESC-NSCs in a dose-dependent manner. Left: immunostaining of TUJ1 of NSCs treated for 7 days with DMSO (control) or CB at various concentrations. Scale bar, 100 μm. Right: quantification of total length of neurite network upon CB treatment for 7 days. Values are normalized to control-treated cells (n = 3).

(D) CB (2 μM)-treated fibroblasts form sphere-like structures in suspension. Scale bars, 200 μm.

(E) Kinase selectivity profiling of CB. Orange bars represent kinases inhibited more than 80% at 1 μM.

(F) Single or combined inhibition of CB target kinases by other compounds (targets in parentheses) has no or smaller effect on sphere formation. Graphs show proliferation rate as fold change of initial cell number (left) and mean sphere diameter (right) at day 3 of suspension culture (n = 3). *p < 0.05 compared to DMSO control. +, p < 0.05 for CB compared to single inhibitors.

major targets AMPK, PKA, MSK1, SGK1, ROCK2, and PKGa (Figure 1E). Single inhibitors of these kinases or combinations of inhibitors did not induce similar increase in sphere size and cell number as CB (Figure 1F). However, compounds H89 and Y27632, both inhibiting ROCK2, also induced a significant increase in sphere diameter compared to control-treated cells but did not induce an increase in proliferation rate. Thus, the effects of CB on sphere formation and cell proliferation apparently depend on the inhibition of a combination of distinct signaling pathways.

Conversion of Fibroblasts into Transient Neural Precursors

Based on sphere formation as initial step, we established an optimized protocol to induce a transient precursor (tP) phenotype in postnatal fibroblasts (Figure 2A) tested negative for neural crest and Schwann cell markers (Figures S1A–S1C). First, fibroblasts were treated with the histone deacetylase (HDAC) inhibitor valproic acid (VPA). VPA is known to enhance reprogramming and transdifferentiation processes (Huangfu et al., 2008; Tursun et al., 2011) and increased the effect of CB on sphere size in our protocol (Figure 2B). VPA treatment was followed by induction of a neural precursor fate by CB treatment in neural stem cell medium. The resulting cells were expanded and additionally treated with synergistic inhibitors of BMP (Noggin), TGF-β (SB431542), and GSK3β (CP21, Roche Compound) signaling. This strategy is known to enhance gene-transfer-dependent neural conversion of fibroblasts (Ladewig et al., 2012). Then, spheres were plated on polyornithine-laminin (POL) and transferred to differentiation medium. Sphere attachment was observed within 2 hr after plating, and cells soon started to migrate out of spheres. In contrast, if spheres had been generated using inhibitors of single CB targets, sphere attachment was highly impaired and no or only poor migration of cells was observed (Figure S2). During physiological NC development, laminin represents one of the key ECM components mediating migration and survival of NC cells (Bronner-Fraser, 1986; Desban et al., 2006). Thus, the capacity to attach rapidly and migrate on laminin indicates that CB-treated cells have adopted some NC features.

Twenty-four hours after attachment, cells stained positive for neuroepithelial markers SOX1 and NESTIN but did not express neural crest markers. No expression of SOX2 was observed indicating the absence of neural stem cells (Figure 2C). One week later (d18), cells expressed neural crest markers CD271, SNAI1, SOX10, FOXD3, and PAX3 suggesting they had adopted some features of NC cells (Figures 2D and 2E). Loss of fibroblast identity was indicated by downregulation of the fibroblast surface marker CD29 (Figure 2E). When cultured in specific differentiation media, tPs formed adipocytes, smooth muscle cells, and chondrocytes suggesting a multipotent differentiation capacity (Figures 2F–2H). To exclude the possibility that the induced tPs originated from rare mesenchymal stem cells (MSCs) in the initial fibroblasts, we tested both fibroblasts and tPs for expression of the MSC marker CD146 (Halfon et al., 2011). No CD146-positive cells were detected in the initial fibroblast population or in tPs (Figures S1D and S1E).

Differentiation into Induced Schwann Cells

To induce Schwann cell formation, tPs were cultured in differentiation medium for 3–4 weeks. After an initial proliferation phase during the tP stage, cell numbers decreased about 50% and then remained constant until the end of the experiment (Figure S3A). After 4 weeks, cells expressed Schwann cell markers PLP, EGR2 (also known as KROX20), S100B, GALC, and GFAP (Figures 3A–3E, S3B, and S3C) (Bhatheja and Field, 2006; Jessen and Mirsky, 2005). Quantification of cells expressing the Schwann cell marker PLP (Griffiths et al., 1995; Kamholz et al., 1992) revealed that more than 60% of cells had transdifferentiated into induced Schwann cells (iSCs) (Figure 3E). Cells stained negative for the fibroblast marker HMMR and the neuron marker MAP2 indicating the absence of fibroblast and neurons, respectively (Figures S3D and S3E).

To analyze the conversion process on the molecular level, genome-wide gene expression profiling was performed at different time points and with primary Schwann cells. Principal component analysis (PCA) revealed a clear difference between fibroblasts and tPs on the one hand and primary and induced Schwann cells on the other hand, which are more similar to each other than to fibroblasts (Figure 3F). This similarity of primary to induced Schwann cells is also reflected by the high Pearson correlation coefficient for all expressed genes ($r = 0.93$). Gene set enrichment analysis (GSEA) revealed significant upregulation of several biological processes corresponding to Schwann cell functions like extracellular matrix organization, NCAM signaling for neurite outgrowth, Notch signaling, or immune response signaling pathways (Figure 3G; Table S2) (Kidd et al., 2013). These networks were also activated in primary Schwann cells further supporting the Schwann cell identity of iSCs (Table S2). In addition, gene expression profiling showed that iSCs produced several neurotrophic factors for neuronal survival, regeneration, and axonal outgrowth (Figure S3H) (Raivich and Makwana, 2007). Gene sets associated with mitotic cell division were downregulated, which is consistent with the transition from proliferative fibroblasts and precursors into postmitotic Schwann cells (Figures 3G and S3G; Table S2).

It has been shown that so-called skin-derived precursors (Toma et al., 2005) show NC stem cell properties and can give rise to Schwann cells (Fernandes et al., 2004; McKenzie

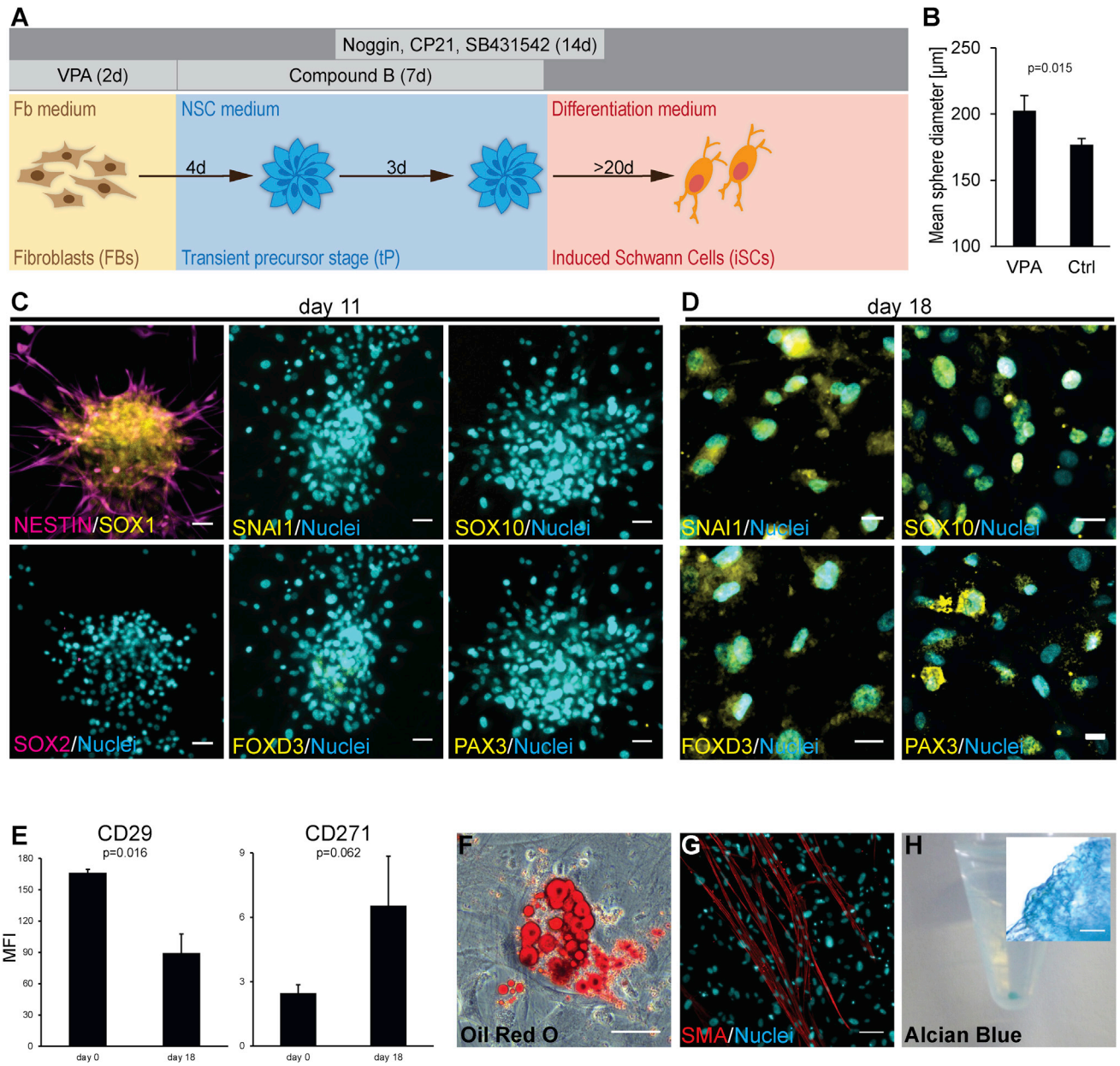

Figure 2. Conversion of Human Fibroblasts into a Transient Neural Precursor Stage

(A) Scheme of experimental setup for conversion into induced Schwann cells.

(B) Pretreatment with valproic acid (VPA) results in increased sphere size. Columns show mean sphere diameter ± SD at day 3 of suspension culture (n = 4).

(C) Secondary spheres at day 11 with bipolar cells growing out of spheres. Cells express neural plate markers SOX1 and NESTIN (top left). No expression of NSC marker SOX2 and of neural crest markers SNAI1, SOX10, FOXD3, and PAX3 was detected. Scale bars, 50 µm.

(D) At day 18, cells express neural crest markers SNAI1, SOX10, FOXD3, and PAX3. Scale bars, 20 µm.

(E) Flow cytometry of precursors (d18) and fibroblasts (d0) revealed downregulation of fibroblast marker CD29 and upregulation of neural crest marker CD271. Panels show quantification of mean fluorescence intensity (MFI) (n = 3).

(F–H) Nonneural differentiation of transient precursors. (F) Adipocyte formation analyzed by oil red O staining. (G) Formation of SMA^+ smooth muscle cells. (H) Formation of chondrocytes analyzed by Alcian blue staining. Inset shows closeup of chondrogenic pellet. Scale bars, 50 (F), 100 (G), and 20 µm (H, inset).

See also Figure S1 and S2.

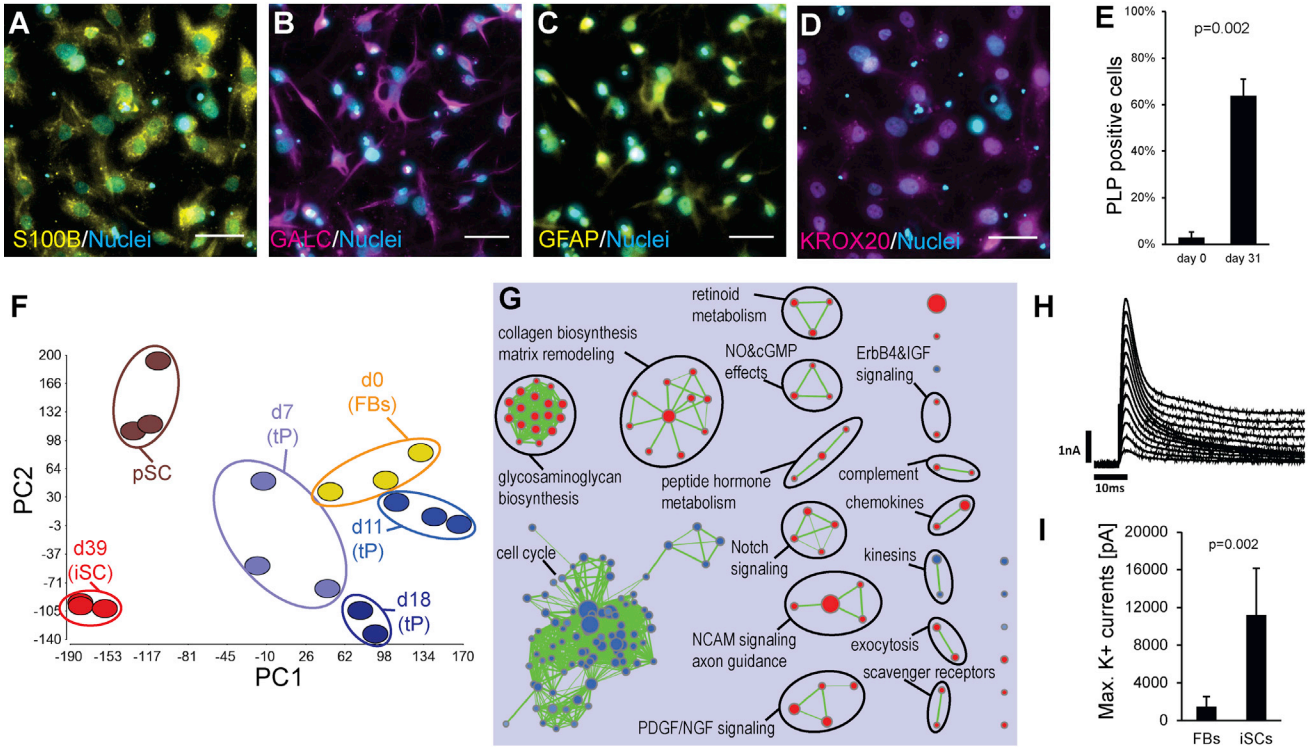

Figure 3. Differentiation of Transient Precursors into Induced Schwann Cells

(A–D) iSCs express Schwann cell markers. Scale bars, 50 μm.

(E) Quantification of PLP-positive cells at d31. Few PLP-positive fibroblasts are due to background signal (n = 3).

(F) Principal component analysis of whole-transcriptome expression profiles from fibroblasts (d0), transdifferentiated cells at d7 (early tP), d11 (early tP), d18 (late tP), d39 (iSCs), and primary Schwann cells (pSCs). Principal component 1 (x axis) accounts for 27.4% and principal component 2 (y axis) accounts for 16.5% of the variation of the data set. Each stage is represented by at least two data points derived from independent experiments. The clustered transcriptomic profiles at day 39 suggest the robustness of the protocol.

(G) Enrichment map of gene sets for cellular signaling pathways (Reactome/NCI Nature PID) derived from GSEA comparing iSCs (d39) with fibroblasts (d0). Red nodes represent gene sets enriched in iSCs, whereas blue nodes represent gene sets enriched in fibroblasts. Nodes are grouped and annotated by their similarity according to related gene sets. Cluster of functionally related nodes were summarized and annotated using WordCloud (n = 3).

(H) Whole patch-clamp analysis of iSCs. Voltage-dependent current obtained from a −70 to +40 mV in 10 mV increasing steps protocol from a holding potential Vh = −80 mV. Absence of early inward current confirms the deficiency of voltage-dependent Na^+ channels, whereas the outward component is consistent with the presence of voltage-dependent K^+ channels.

(I) Maximal voltage-dependent K^+ currents are significantly higher in iSCs than in fibroblasts. Columns show means ± SD of different cells (FBs: n = 12; iSCs: n = 7) measured in two independent experiments.

See also Figure S3 and Table S2.

et al., 2006). To exclude that iSCs originated from skin-derived precursors, depletion of CD271-positive cells was performed in the initial fibroblast population using MACS. CD271-depleted fibroblasts converted into tPs and further into iSCs with no difference in time course or efficiency compared to unsorted fibroblasts (Figures S3I–S3Q). These results suggest that indeed iSCs originated from fibroblasts that converted toward another phenotype, albeit the possibility that rare skin-derived precursors differentiated into Schwann cells cannot be completely excluded.

Functional Features of Induced Schwann Cells

To analyze iSC functionality, we first tested excitability of iSCs performing whole patch-clamp recordings. Brief depolarizing current pulses of increasing intensity did not evoke action potentials. However, upon 100 ms voltage-step pulses from −70 to +40 mV in 10 mV steps increments, a sustained outward current component was observed indicating the presence of voltage-dependent K^+ channels, a known feature of Schwann cells (Baker, 2002). K^+ currents were significantly larger in iSCs compared to untreated fibroblasts (Figures 3H, 3I, and S3F).

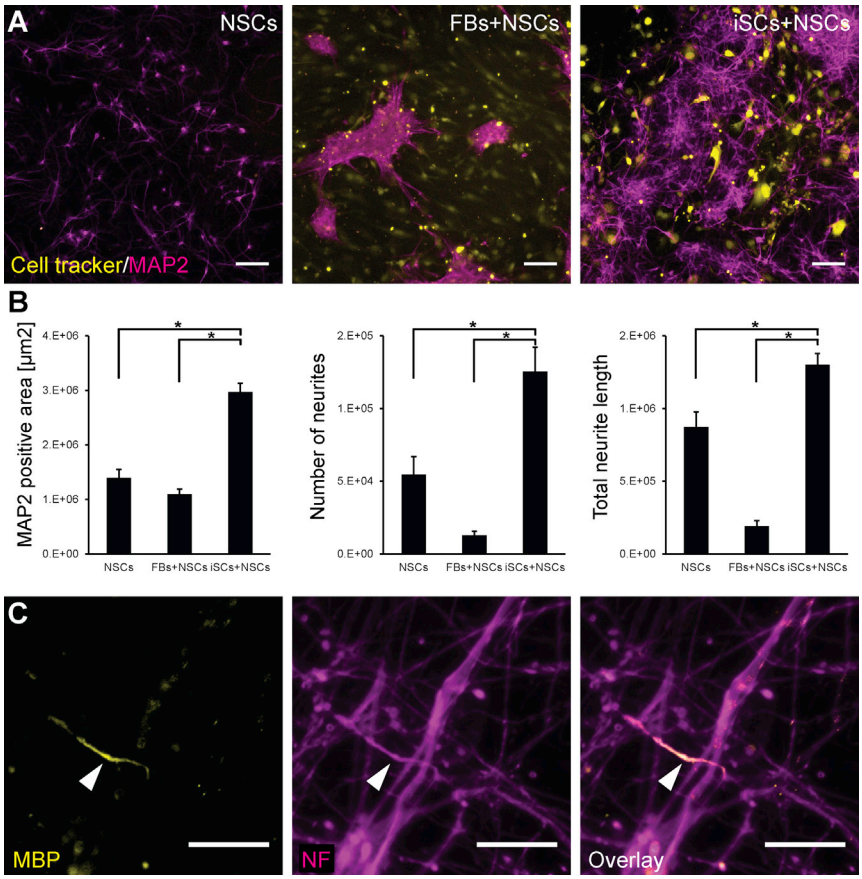

Figure 4. Functionality of iSCs in Coculture with Neuronal Cells

(A) Culture of NSC-derived neurons alone, on cell tracker-labeled fibroblasts and iSCs, respectively. Scale bars, 100 µm.

(B) NSC-neurons cultured with iSCs form a more dense and branched network analyzed by MAP2-stained area, neurite number, and total neurite length (n = 3). *p < 0.05.

(C) Coculture of iSCs with primary rat DRG neurons. Some iSCs form single myelinated fragments (arrowhead) detected by colocalization of MBP staining (yellow) and neurofilament (NF) staining (magenta). Scale bars, 20 µm.

See also Figure S4.

To analyze neuroprotective functionality of iSCs, cells were cocultured with neurons differentiated from human embryonic stem cell (ESC)-derived neural stem cells (NSC-neurons). As control, NSC-neurons were plated on POL or untreated fibroblasts. NSC-neurons plated on fibroblasts aggregated in dense clusters whereas cocultured iSCs and NSC-neurons formed a dense, multicellular network (Figures 4A and S4). MAP2 staining confirmed that NSC-neurons cultured with iSCs formed a more branched neurite network than NSC-neurons grown alone or with fibroblasts (Figure 4B). Moreover, total number of neurons was also increased in coculture with iSCs (Figure S4J). These results suggest that iSCs are capable to enhance neuronal survival, differentiation, and neurite network formation.

To test if iSCs are capable of myelination, iSCs were cocultured with primary rat dorsal root ganglia neurons (DRGs). After 3 weeks, myelinated axon segments could be observed further confirming the functionality of iSCs (Figure 4C). The low frequency of myelinated fragments (five to ten fragments/96 well) might be due to species differences between iSCs and neurons. This observation is in line with previous studies showing that human Schwann cells had a markedly reduced efficacy to myelinate rat sensory neurons compared to primary rat Schwann cells (Lehmann et al., 2012).

DISCUSSION

In recent years, numerous studies reporting reprogramming or transdifferentiation of somatic cells have shown that even in terminally differentiated cells fate plasticity can be evoked and that transition to other cell types, even across germ-layer boundaries, is still possible.

Here, we present an approach to transdifferentiate human fibroblasts via a transient precursor stage into Schwann cells that does not depend on ectopic gene expression but is based on chemical modification of defined signaling pathways. Such gene-free, chemical-based conversion strategies allow the generation of cells without genetic modifications and furthermore can be very tightly controlled by altering concentrations or duration of small molecule treatment.

In our approach, conversion to Schwann cells was induced by sequential treatment with defined compounds. First, a brief VPA treatment step probably resulted in an

erase of epigenetic signatures making cells more amenable for cell-fate changing signals—a process that may also be involved in gene-free iPS generation or transdifferentiation into endodermal cells (Hou et al., 2013; Pennarossa et al., 2013). Fate determination toward transient precursors was achieved by treatment with CB inhibiting AMPK, MSK1, PKA, ROCK2, PKGa, and SGK1. Several studies of these signaling pathways allow assumptions regarding the mechanistic regulation of the conversion process. Because upregulation of SGK1 correlates with cell death in neurodegenerative disease (Schoenebeck et al., 2005), its inhibition might enhance the survival of cells that converted toward a neural fate. Moreover, CB might abolish a metabolic barrier mediated by AMPK signaling, which is known to prevent reprogramming processes (Vazquez-Martin et al., 2012).

ROCK2 inhibition evokes a proliferative, stem cell-like phenotype (Terunuma et al., 2010), promotes emigration of neural crest cells (Groysman et al., 2008), and has neuroprotective effects (Ding et al., 2009). These effects might also support fibroblast conversion into neural precursors and iSCs.

Additionally, our approach included small molecule-based inhibition of TGF-β, BMP, and GSK3 signaling, a strategy known to direct differentiation of ESCs to neuroepithelial and/or neural crest fates (Chambers et al., 2009; Menendez et al., 2011).

Altogether, this study shows as proof of principle that conversion of fibroblasts toward a neural cell fate can be achieved solely by small molecule treatment. We identified CB as potent compound to induce neural cell identity and developed a CB-based approach to efficiently generate Schwann cells without any genetic modifications. Compared to existing Schwann cell sources like derivation from pluripotent stem cells (Liu et al., 2012) or as primary cells (Casella et al., 1996), chemical-based conversion is more cost effective and easier to control and to standardize. Because Schwann cells play an important role in development, homeostasis, and diseases of the peripheral nervous system (Bhatheja and Field, 2006), we suggest that iSCs could represent useful tools to analyze Schwann cell functions or pathophysiology in vitro and to develop cellular interaction models allowing to study disease mechanisms in neuron-Schwann cell coculture.

EXPERIMENTAL PROCEDURES

Details are provided as Supplemental Experimental Procedures.

Cell Culture

SCC058 foreskin fibroblasts (Millipore) were seeded in low serum FibroGro (Millipore) containing 1 mM Valproic acid (VPA, Sigma). Cells were treated for 2 days with 1 mM VPA and 6 μg/ml polybrene (Millipore) and subsequently transferred to low attachment plates in NSC medium for sphere formation. After 4 days, spheres were dissociated, and cells were seeded in low attachment plates in NSC medium supplemented with inhibitor mix consisting of 500 ng/ml Noggin (PeproTech), 10 μM SB431452 (Tocris Bioscience), and 1 μM CP21 (Roche, GSK3 inhibitor, published elsewhere). After 3 days, secondary spheres were seeded on polyornithine-laminin (POL)-coated dishes. After attachment (24 hr), medium was replaced with neural differentiation medium. Every other day, 50% of medium was exchanged. For the first 7 days of differentiation, medium was supplemented with inhibitor mix. MACS depletion of CD271-positive cells from the initial fibroblasts was performed using a CD271 Microbead kit (Miltenyi).

For adipocyte and smooth muscle cell differentiation, secondary spheres were plated on growth factor reduced matrigel. After 24 hr, medium was changed to adipocyte differentiation medium. Medium was changed every other day. After 4 weeks, cells were fixed with 4% paraformaldehyde (PFA) and stained with oil red O or anti-SMA.

For chondrogenesis, secondary spheres were cultured as pellet in chondrocyte differentiation medium. After 4 weeks, the pellet was fixed with 4% PFA and analyzed by Alcian blue staining.

Embryonic stem cell-derived neural stem cells (NSCs) were generated as previously described (Chambers et al., 2009). NSCs were cultured on POL in N2B27 supplemented with basic fibroblast growth factor (10 ng/ml), epidermal growth factor (10 ng/ml), and brain derived neurotrophic factor (20 ng/ml).

For iSC/NSC neuron coculture, NSCs were cultured in differentiation medium for 13 days and then seeded in differentiation medium on POL only, fibroblasts, or iSCs at 120,000 NSC-neurons/12 well. Fibroblasts and iSCs had been previously labeled with CFSE cell tracker (Invitrogen, 10 μM for 20 min). Every other day, 50% of medium was exchanged. Cells were fixed with 4% PFA at day 13 of coculture.

For iSC/rat DRG coculture, embryonic rat DRG neurons (Lonza) were seeded on poly-D-Lysine-laminin-coated plates and cultured at 37°C, 5% CO_2 in PNGM medium (Lonza) supplemented with 100 ng/ml NGF (PeproTech). To eliminate rat glial cells, cultures were treated with 17.5 μg/ml uridine and 7.5 μg/ml 5-fluoro-2-deoxyuridine (both Sigma) for at least 7 days. Then, iSCs (day 21) were seeded on DRG cultures at 30,000 cells/cm^2. Cultures were maintained in PNGM medium supplemented with 100 ng/ml NGF with 50% medium exchange every other day. At day 4 of coculture, myelination was induced by adding 50 μg/ml ascorbic acid to the medium.

Human primary Schwann cells (Sciencell) were cultured on poly-L-lysine coated dishes in Schwann cell medium (Sciencell).

Kinase Selectivity Profiling

Kinase selectivity profiling was performed using ProfilerPro Kinase Kits from Caliper (PerkinElmer) according to the manufacturer's instructions.

Genome-wide Gene Expression Analysis

RNA samples were processed for microarray expression profiling using the Affymetrix HG-U133_plus_2 platform. Data analysis was performed using Partek Genomics Suite 6.6 (Partek) and Gene Set Enrichment Analysis.

Statistics

Data are presented as mean ± SD. Statistical significance was tested with Student's t test. The number of independent experiments is given as "n."

ACCESSION NUMBERS

The microarray data have been deposited at the NCBI Gene Expression Omnibus (GEO) under the accession number GSE59125.

SUPPLEMENTAL INFORMATION

Supplemental Information includes Supplemental Experimental Procedures, four figures, and two tables and can be found with this article online at http://dx.doi.org/10.1016/j.stemcr.2014.07.014.

ACKNOWLEDGMENTS

This work was supported by the Roche Postdoctoral Fellowship program. We thank K. Christensen, S. Schlicht, S. Zimmermann, and W. Keilholz for technical assistance. The authors E.C.T., T.H., R.H., F.K., C.N., N.F., P.P., R.J., S.J.Z., H.H.T., M.G., and R.I. are employees of F. Hoffmann-La Roche, Ltd. Small amounts of CB can be made available upon request.

Received: November 1, 2013
Revised: July 30, 2014
Accepted: July 30, 2014
Published: September 11, 2014

REFERENCES

Baker, M.D. (2002). Electrophysiology of mammalian Schwann cells. Prog. Biophys. Mol. Biol. *78*, 83–103.

Bhatheja, K., and Field, J. (2006). Schwann cells: origins and role in axonal maintenance and regeneration. Int. J. Biochem. Cell Biol. *38*, 1995–1999.

Bronner-Fraser, M. (1986). An antibody to a receptor for fibronectin and laminin perturbs cranial neural crest development in vivo. Dev. Biol. *117*, 528–536.

Casella, G.T., Bunge, R.P., and Wood, P.M. (1996). Improved method for harvesting human Schwann cells from mature peripheral nerve and expansion in vitro. Glia *17*, 327–338.

Chambers, S.M., Fasano, C.A., Papapetrou, E.P., Tomishima, M., Sadelain, M., and Studer, L. (2009). Highly efficient neural conversion of human ES and iPS cells by dual inhibition of SMAD signaling. Nat. Biotechnol. *27*, 275–280.

Desban, N., Lissitzky, J.C., Rousselle, P., and Duband, J.L. (2006). alpha1beta1-integrin engagement to distinct laminin-1 domains orchestrates spreading, migration and survival of neural crest cells through independent signaling pathways. J. Cell Sci. *119*, 3206–3218.

Ding, J., Yu, J.Z., Li, Q.Y., Wang, X., Lu, C.Z., and Xiao, B.G. (2009). Rho kinase inhibitor Fasudil induces neuroprotection and neurogenesis partially through astrocyte-derived G-CSF. Brain Behav. Immun. *23*, 1083–1088.

Dontu, G., Abdallah, W.M., Foley, J.M., Jackson, K.W., Clarke, M.F., Kawamura, M.J., and Wicha, M.S. (2003). In vitro propagation and transcriptional profiling of human mammary stem/progenitor cells. Genes Dev. *17*, 1253–1270.

Fernandes, K.J., McKenzie, I.A., Mill, P., Smith, K.M., Akhavan, M., Barnabé-Heider, F., Biernaskie, J., Junek, A., Kobayashi, N.R., Toma, J.G., et al. (2004). A dermal niche for multipotent adult skin-derived precursor cells. Nat. Cell Biol. *6*, 1082–1093.

Griffiths, I.R., Dickinson, P., and Montague, P. (1995). Expression of the proteolipid protein gene in glial cells of the post-natal peripheral nervous system of rodents. Neuropathol. Appl. Neurobiol. *21*, 97–110.

Groysman, M., Shoval, I., and Kalcheim, C. (2008). A negative modulatory role for rho and rho-associated kinase signaling in delamination of neural crest cells. Neural Dev. *3*, 27.

Halfon, S., Abramov, N., Grinblat, B., and Ginis, I. (2011). Markers distinguishing mesenchymal stem cells from fibroblasts are down-regulated with passaging. Stem Cells Dev. *20*, 53–66.

Hou, P., Li, Y., Zhang, X., Liu, C., Guan, J., Li, H., Zhao, T., Ye, J., Yang, W., Liu, K., et al. (2013). Pluripotent stem cells induced from mouse somatic cells by small-molecule compounds. Science *341*, 651–654.

Huangfu, D., Maehr, R., Guo, W., Eijkelenboom, A., Snitow, M., Chen, A.E., and Melton, D.A. (2008). Induction of pluripotent stem cells by defined factors is greatly improved by small-molecule compounds. Nat. Biotechnol. *26*, 795–797.

Jessen, K.R., and Mirsky, R. (2005). The origin and development of glial cells in peripheral nerves. Nat. Rev. Neurosci. *6*, 671–682.

Kamholz, J., Sessa, M., Scherer, S., Vogelbacker, H., Mokuno, K., Baron, P., Wrabetz, L., Shy, M., and Pleasure, D. (1992). Structure and expression of proteolipid protein in the peripheral nervous system. J. Neurosci. Res. *31*, 231–244.

Kidd, G.J., Ohno, N., and Trapp, B.D. (2013). Biology of Schwann cells. Handb. Clin. Neurol. *115*, 55–79.

Ladewig, J., Mertens, J., Kesavan, J., Doerr, J., Poppe, D., Glaue, F., Herms, S., Wernet, P., Kögler, G., Müller, F.J., et al. (2012). Small molecules enable highly efficient neuronal conversion of human fibroblasts. Nat. Methods *9*, 575–578.

Lehmann, H.C., Chen, W., Mi, R., Wang, S., Liu, Y., Rao, M., and Höke, A. (2012). Human Schwann cells retain essential phenotype characteristics after immortalization. Stem Cells Dev. *21*, 423–431.

Liu, Q., Spusta, S.C., Mi, R., Lassiter, R.N., Stark, M.R., Höke, A., Rao, M.S., and Zeng, X. (2012). Human neural crest stem cells derived from human ESCs and induced pluripotent stem cells: induction, maintenance, and differentiation into functional schwann cells. Stem Cells Transl. Med. *1*, 266–278.

McKenzie, I.A., Biernaskie, J., Toma, J.G., Midha, R., and Miller, F.D. (2006). Skin-derived precursors generate myelinating Schwann cells for the injured and dysmyelinated nervous system. J. Neurosci. *26*, 6651–6660.

Menendez, L., Yatskievych, T.A., Antin, P.B., and Dalton, S. (2011). Wnt signaling and a Smad pathway blockade direct the differentiation of human pluripotent stem cells to multipotent neural crest cells. Proc. Natl. Acad. Sci. USA *108*, 19240–19245.

Pennarossa, G., Maffei, S., Campagnol, M., Tarantini, L., Gandolfi, F., and Brevini, T.A. (2013). Brief demethylation step allows the conversion of adult human skin fibroblasts into insulin-secreting cells. Proc. Natl. Acad. Sci. USA *110*, 8948–8953.

Raivich, G., and Makwana, M. (2007). The making of successful axonal regeneration: genes, molecules and signal transduction pathways. Brain Res. Brain Res. Rev. *53*, 287–311.

Schoenebeck, B., Bader, V., Zhu, X.R., Schmitz, B., Lübbert, H., and Stichel, C.C. (2005). Sgk1, a cell survival response in neurodegenerative diseases. Mol. Cell. Neurosci. *30*, 249–264.

Stuhlmiller, T.J., and García-Castro, M.I. (2012). Current perspectives of the signaling pathways directing neural crest induction. Cell. Mol. Life Sci. *69*, 3715–3737.

Terunuma, A., Limgala, R.P., Park, C.J., Choudhary, I., and Vogel, J.C. (2010). Efficient procurement of epithelial stem cells from human tissue specimens using a Rho-associated protein kinase inhibitor Y-27632. Tissue Eng. Part A *16*, 1363–1368.

Toma, J.G., McKenzie, I.A., Bagli, D., and Miller, F.D. (2005). Isolation and characterization of multipotent skin-derived precursors from human skin. Stem Cells *23*, 727–737.

Tropepe, V., Coles, B.L., Chiasson, B.J., Horsford, D.J., Elia, A.J., McInnes, R.R., and van der Kooy, D. (2000). Retinal stem cells in the adult mammalian eye. Science *287*, 2032–2036.

Tursun, B., Patel, T., Kratsios, P., and Hobert, O. (2011). Direct conversion of C. elegans germ cells into specific neuron types. Science *331*, 304–308.

Vazquez-Martin, A., Vellon, L., Quirós, P.M., Cufí, S., Ruiz de Galarreta, E., Oliveras-Ferraros, C., Martin, A.G., Martin-Castillo, B., López-Otín, C., and Menendez, J.A. (2012). Activation of AMP-activated protein kinase (AMPK) provides a metabolic barrier to reprogramming somatic cells into stem cells. Cell Cycle *11*, 974–989.

Vierbuchen, T., and Wernig, M. (2011). Direct lineage conversions: unnatural but useful? Nat. Biotechnol. *29*, 892–907.

Stem Cell Reports, Volume *3*

Supplemental Information

Chemical Conversion of Human Fibroblasts into Functional Schwann Cells

Eva C. Thoma, Claudia Merkl, Tobias Heckel, Rachel Haab, Frederic Knoflach, Corinne Nowaczyk, Nicholas Flint, Ravi Jagasia, Sannah Jensen Zoffmann, Hoa Hue Truong, Pascal Petitjean, Sebastian Jessberger, Martin Graf, and Roberto Iacone

Figure S1

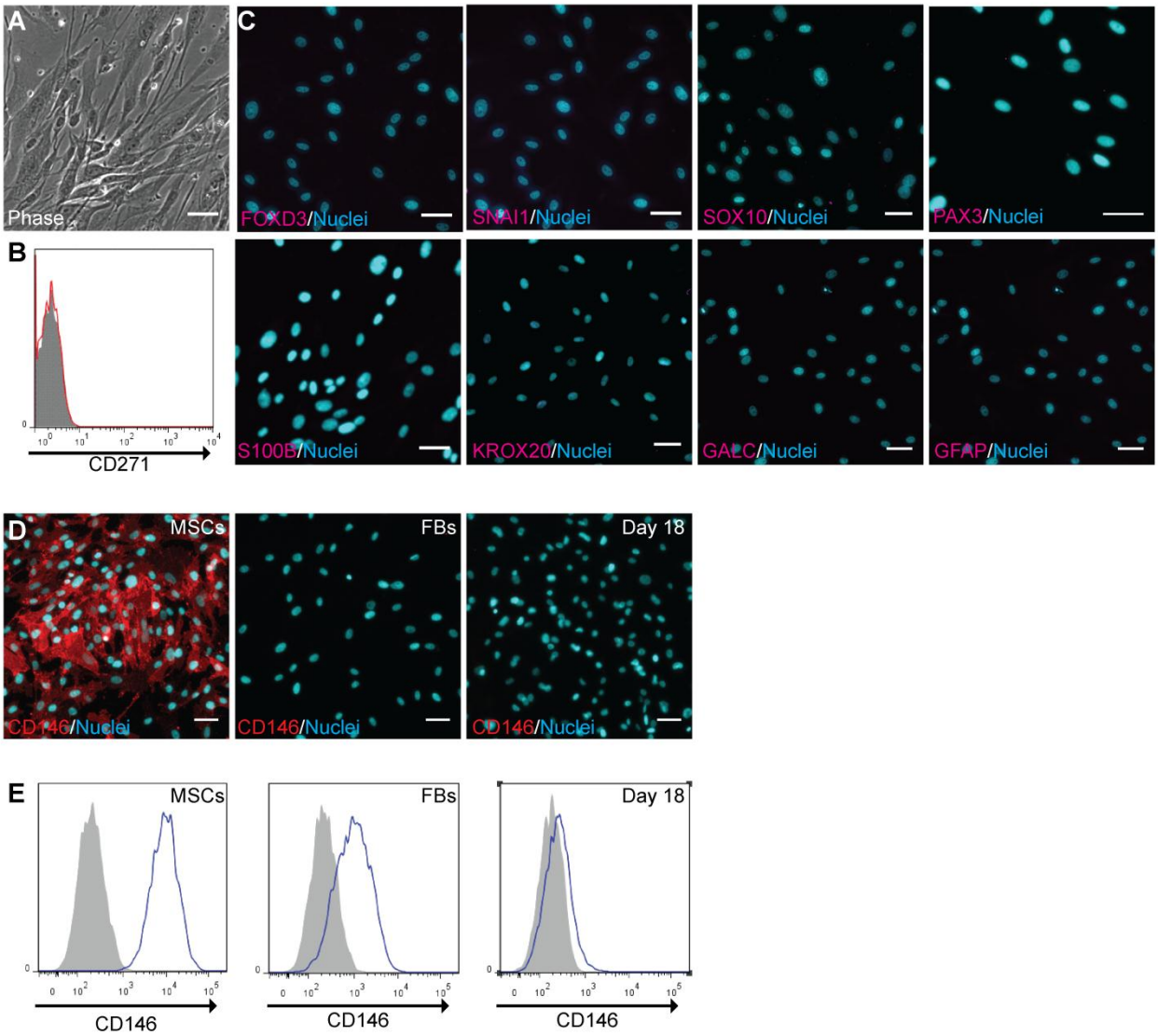
A
Phase
C
FOXD3/Nuclei
SNAI1/Nuclei
SOX10/Nuclei
PAX3/Nuclei
B
CD271
S100B/Nuclei
KROX20/Nuclei
GALC/Nuclei
GFAP/Nuclei
D
MSCs
FBs
Day 18
CD146/Nuclei
CD146/Nuclei
CD146/Nuclei
E
MSCs
FBs
Day 18
CD146
CD146
CD146

Figure S2

A

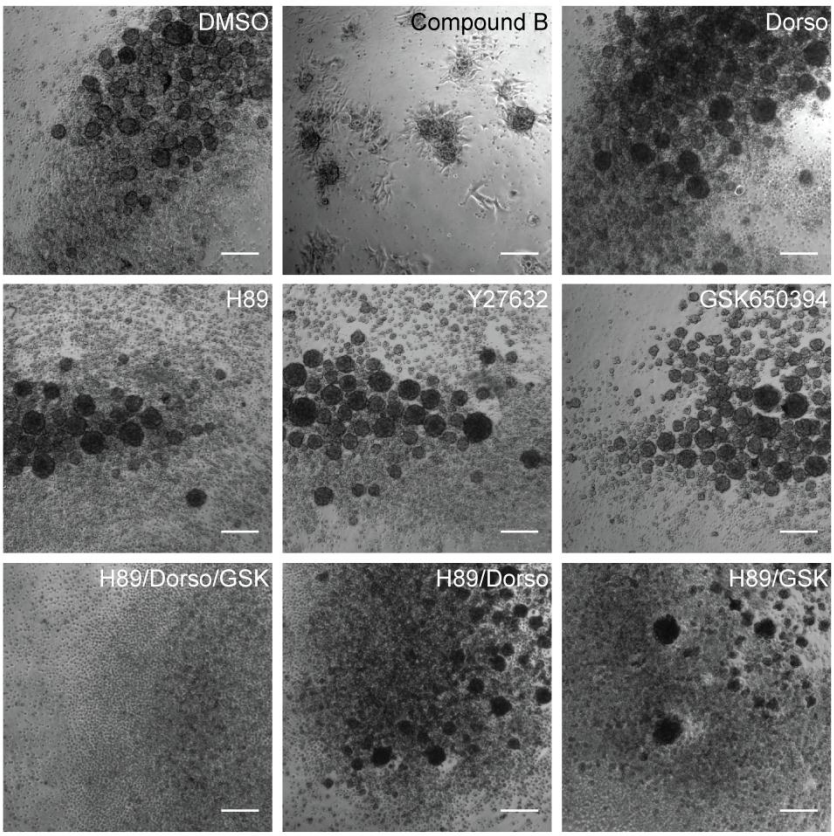
DMSO
Compound B
Dorso
H89
Y27632
GSK650394
H89/Dorso/GSK
H89/Dorso
H89/GSK

B

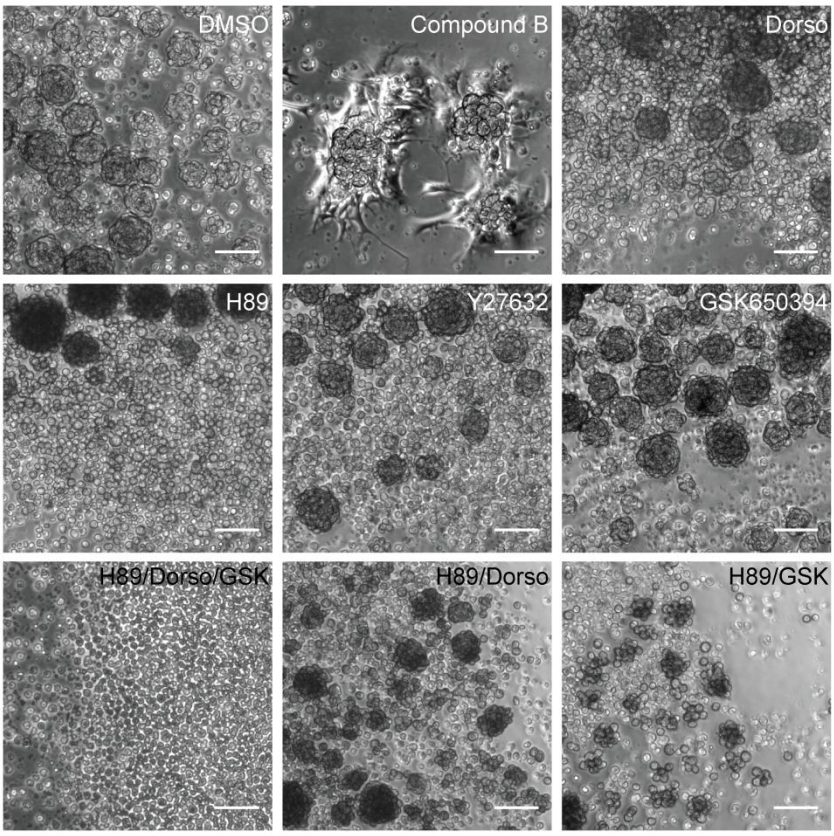
DMSO
Compound B
Dorso
H89
Y27632
GSK650394
H89/Dorso/GSK
H89/Dorso
H89/GSK

Figure S3

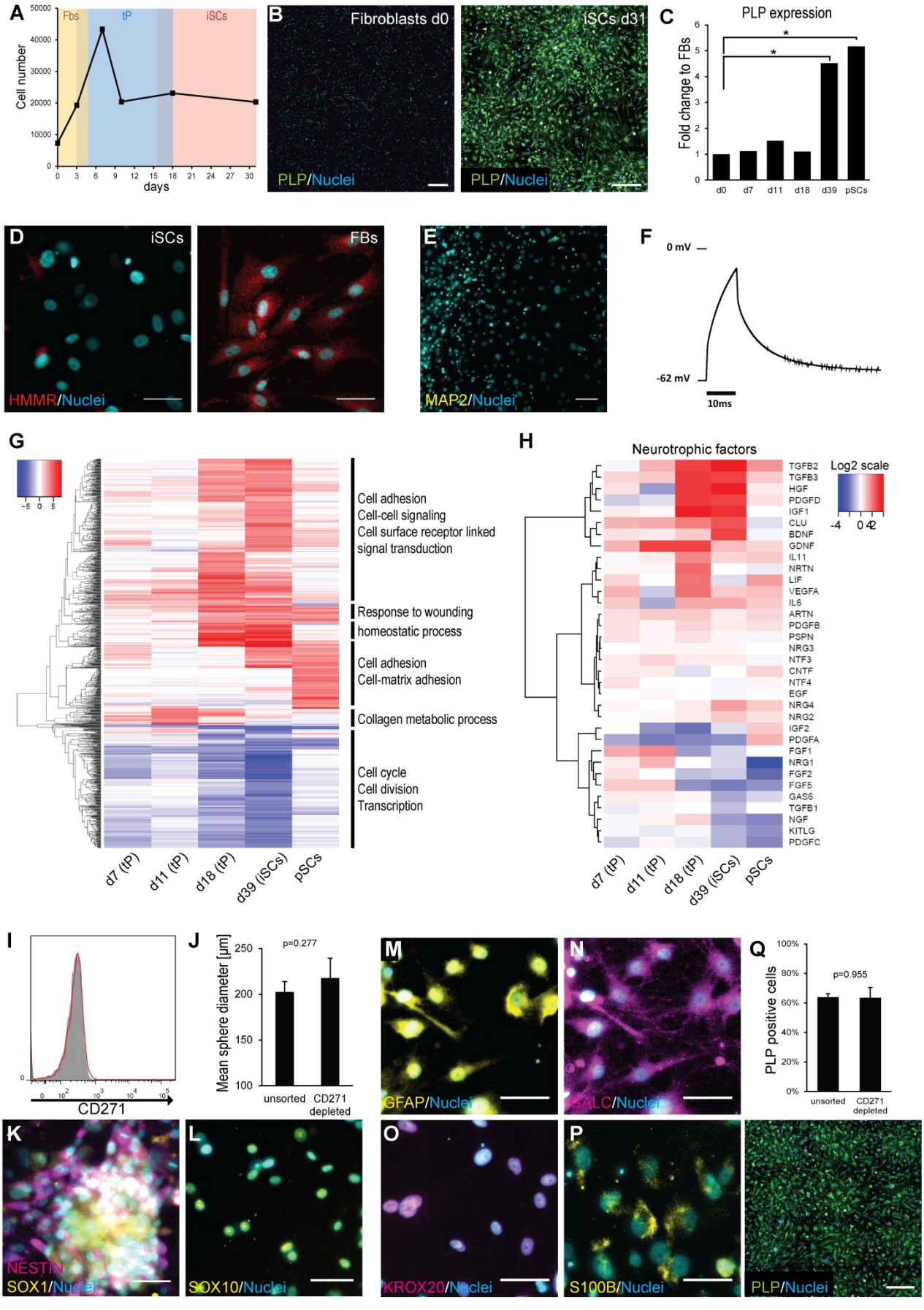
A
Fbs
tP
iSCs
Cell number
days
B
Fibroblasts d0
PLP/Nuclei
iSCs d31
PLP/Nuclei
C
PLP expression
Fold change to FBs
d0
d7
d11
d18
d39
pSCs
D
iSCs
HMMR/Nuclei
FBs
E
MAP2/Nuclei
F
0 mV
-62 mV
10ms
G
Cell adhesion
Cell-cell signaling
Cell surface receptor linked signal transduction
Response to wounding
homeostatic process
Cell adhesion
Cell-matrix adhesion
Collagen metabolic process
Cell cycle
Cell division
Transcription
d7 (tP)
d11 (tP)
d18 (tP)
d39 (iSCs)
pSCs
H
Neurotrophic factors
Log2 scale
TGFB2
TGFB3
HGF
PDGFD
IGF1
CLU
BDNF
GDNF
IL11
NRTN
LIF
VEGFA
IL6
ARTN
PDGFB
PSPN
NRG3
NTF3
CNTF
NTF4
EGF
NRG4
NRG2
IGF2
PDGFA
FGF1
NRG1
FGF2
FGF5
GAS6
TGFB1
NGF
KITLG
PDGFC
I
CD271
J
Mean sphere diameter [µm]
p=0.277
unsorted
CD271 depleted
M
GFAP/Nuclei
N
GALC/Nuclei
Q
PLP positive cells
p=0.955
unsorted
CD271 depleted
K
NESTIN
SOX1/Nuclei
L
SOX10/Nuclei
O
KROX20/Nuclei
P
S100B/Nuclei
PLP/Nuclei

Figure S4

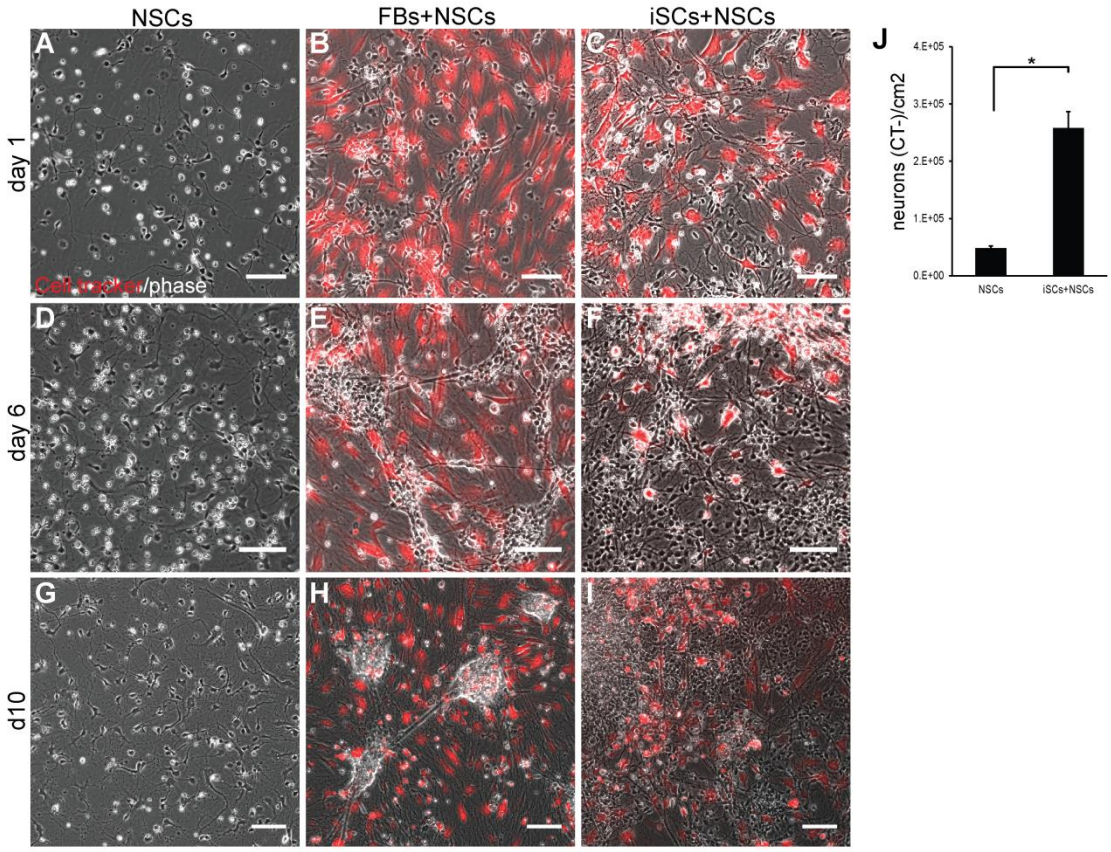
NSCs
FBs+NSCs
iSCs+NSCs
day 1
day 6
d10
A
B
C
D
E
F
G
H
I
Cell tracker/phase
J
neurons (CT-)/cm2
4.E+05
3.E+05
2.E+05
1.E+05
0.E+00
*
NSCs
iSCs+NSCs

Supplemental Figure Legends

Figure S1, related to Figure 2: Characterization of human fibroblasts used for iSC generation. (A-C) Human fibroblasts do not express neural crest or Schwann cell markers. (A) Phase contrast image of fibroblasts. Scale bar: 50µm. (B) Flow cytometry analysis of initial fibroblast population. No CD271 positive cells were detected. Unstained control is shown as grey filled graph. (C) Immunostaining for neural crest and Schwann cell markers. Nuclei were visualized with Hoechst staining. Scale bars: 50µm. (D, E) Fibroblast cultures and induced transient precursors do not contain mesenchymal stem cells (MSCs). Expression analysis of MSC marker CD146 by immunostaining (D) and flow cytometry (E). MSCs derived from embryonic stem cells were used as positive control. Scale bars in D: 50µm.

Figure S2, related to Figure 2: Attachment of spheres to laminin substrate is mediated by Compound B treatment. Low magnification (A) and close up (B) view of secondary spheres generated with CB or inhibitors of single CB targets two hours after plating on polyornithine-laminin coated dishes. Only CB treated spheres (top middle) have attached and started to migrate. In control (DMSO) and single inhibitor conditions floating spheres have aggregated in center of wells. Scale bars: 200µm (A), 100µm (B).

Figure S3, related to Figure 3: Formation of induced Schwann cells (iSCs). (A) Schematic growth curve during the transdifferentiation process. Average cell numbers were calculated from at least 3 independent assays. Colored boxes indicate the putative stage of conversion as shown in Fig. 2A. (B) Wide field view of staining for Schwann cell marker PLP of fibroblasts (d0) and iSCs (d31). Few PLP positive fibroblasts are due to background signal. Scale bars: 500µm. (C) Whole transcriptome analysis using ANOVA reveals statistically significant up-regulation of PLP expression during the conversion procedure to a level similar to primary SCs (* $p < 0.05$). Columns show meanfold change values from three independent experiments with exception of $n = 2$ for day 18 cells. (D) Conversion protocol resulted in loss of fibroblast identity. Immunostaining for fibroblast marker HMMR in iSCs at day 25 (left) and untreated fibroblasts (right). Scale bars: 50µm. (E) Conversion protocol did not yield neurons as shown by negative MAP2 staining at day 31. Nuclei were visualized with Hoechst staining. Scale bars: 100µm. (F) Whole patch clamp analysis of iSCs. Membrane responses to depolarizing current pulses injected into iSC. Only a deflection of the membrane potential, but no action potential was detected. (G, H) Global transcriptome analysis during the conversion process. (G) Global heat map of 700 differentially expressed genes between fibroblasts (d0) and transdifferentiated cells at d7 (early tP),

d11 (early tP), d18 (late tP), d39 (iSCs), and primary Schwann cells (pSCs) (>10 fold change and $p < 0.05$ during at least 1 time point). Hierarchical clustering of globally down-regulated genes (blue) and up-regulated genes (red) was performed on Log_2 Fold Changes using the average linkage method and the Euclidean distance metric. GO terms for Biological Processes were used for cluster annotation. For each stage, data from at least two independent assays were analyzed. (H) Heat map showing differential expression of hierarchically clustered neurotrophic factors. Log_2 Fold Changes indicate down-regulation in blue and up-regulation in red. Data from at least two independent experiments are shown. (I-Q) Generation of iSCs after depletion of CD271 positive cells. (I) Flow cytometry of fibroblasts after depletion of CD271 positive cells using stringent MACS procedure. CD271 positive cells have been completely removed. Unstained control is shown as grey filled graph. (J-L) CD271 depletion does not affect sphere formation and conversion to transient progenitor stage. (J) Mean sphere diameter +/- SD at day 3 of suspension culture of unsorted or CD271 depleted fibroblasts (n=4). (K, L) CD271 depleted fibroblasts converting to transient precursor stage expressing SOX1 and NESTIN at day 11 (K), followed by activation of neural crest marker SOX10 at day 18 (L). Scale bars: 50µm. (M-P) CD271 negative fibroblasts convert into iSCs expressing Schwann cell marker proteins. Scale bars 50µm. (Q) Depletion of CD271 positive cells does not influence efficiency of conversion. Quantification of PLP positive cells at d31. (n=3). Lower panel shows wide field view of PLP staining at day 31 of conversion of CD271 depleted cells. Scale bar: 500µm.

Figure S4, related to Figure 4: Co-culture of NSC-derived neurons on POL, cell tracker-labeled fibroblasts or cell tracker-labeled iSCs. (A-I) Overlays of phase contrast images and cell tracker signal (red). NSC-neurons can be identified by characteristic small, dark soma. At day 1, NSC-neurons have attached on all three surfaces (A-C). Prolonged co-culture with fibroblasts led to aggregation of neurons and poor neurite outgrowth (E, H). Co-culture with iSCs resulted in proliferation and formation of a dense, multicellular network (F, I). Scale bars: 100µm. (J) NSC-neurons co-cultured with iSCs show higher cell numbers compared to NSC-neurons cultured alone (n=3). *: $p<0.05$.

Table S1: Examples of recent studies reporting direct conversion of human cell types by ectopic expression of key developmental genes. As there are numerous studies describing direct conversion, several representative reports for different converted cell types (only human cells) were chosen.

Original cell type	Converted cell type	Conversion factors[1]	Efficiency[2]	Duration[3]	Reference
Postnatal or fetal FBs	Neurons	*BRN2, ASCL1, MYT1L, NEUROD*	2-4%	4-5 weeks	(Pang et al., 2011)
Postnatal FBs Adult primary FBs	Neurons	*miR124, BRN2, MYT1L*	Postnatal FBs: 4-8% Adult primary FBs: 1.5-11.2%	30 days	(Ambasudhan et al., 2011)
Foreskin FBs (fFBS) Dermal FBs (dFBs) Adult cardiac FBs (acFBs)	Cardiomyocytes	*GATA4, HAND2, TBX5, MYOCD, miR1, miR133*	fFBs: 20% dFBs: 9.5% acFBs: 12%	4 weeks	(Nam et al., 2013)
Dermal FBs Cardiac FBs	Cardiomyocytes	*GATA4, MEF2C, TBX5, ESRRG, MESP1, MYOCD, ZFPM2*	13% primary FBs: 1-4%	10 weeks	(Fu et al., 2013)
Foreskin FBs	Retinal pigment epithelial-like cells	*CMYC, MITF, OTC2, RAX, CRX*	22%	35 days	(Zhang et al., 2014)
Neonatal FBs	Chondrogenic cells	*CMYC, KLF4, SOX9*	0.25%	14-18 days	(Outani et al., 2013)

1: Minimal combination required for best efficiency
2: Efficiency as determined by marker expression
3: Duration of assay until the appearance of functional features of the converted cells

Table S2: Enrichment of cellular signaling pathways (Reactome/NCI-Nature PID) representing Schwann cell functionality in day 39 induced Schwann Cells (iSCs) and primary Schwann cells (pSCs) in comparison to fibroblasts. Pathway-overrepresentation in Gene Set Enrichment Analysis (GSEA) is indicated by the normalized enrichment score (NES), the statistical significance of the enrichment score is indicated by the nominal p-value, and the probability that the normalized enrichment score represents a false positive finding is indicated by the false discovery rate (FDR) q-value. Note the down-regulation of the cell cycle in iSCs in contrast to primary Schwann Cells.

Legend for references: in this table:

1 (Woodhoo and Sommer, 2008)

2 (Meyer zu Horste et al., 2008)

3 (Ydens et al., 2013)

4 (Raivich and Makwana, 2007)

5 (Bhatheja and Field, 2006)

6 (Higginson et al., 2012)

7 (Woodhoo et al., 2009)

			iSCs (d39)			Primary SCs			
function	**NAME**	**Reactome ID**	**NES**	**NOM p-value**	**FDR q-value**	**NES**	**NOM p-value**	**FDR q-value**	**reference**
collagen biosynthesis	COLLAGEN_BIOSYNTHESIS_AND_MODIFYING_ENZYMES_REACTOME	REACT_121139.2	2.27	>0.0001	>0.0001	1.70	0.0013	0.0448	1
neural cell adhesion networks	NCAM1_INTERACTIONS_REACTOME	REACT_18312.1	2.12	>0.0001	>0.0001	1.74	0.0014	0.0487	4
Immunocompetence of Schwann cells	INTERFERON_ALPHA_BETA_SIGNALING_REACTOME	REACT_25162.1	1.99	>0.0001	0.0006	1.16	0.2321	0.5567	2, 3
extracellular matrix organization	EXTRACELLULAR_MATRIX_ORGANIZATION_REACTOME	REACT_118779.5	2.11	>0.0001	>0.0001	1.83	>0.0001	0.0286	1
neural cell adhesion networks	NCAM_SIGNALING_FOR_NEURITE_OUT_GROWTH_REACTOME	REACT_18334.1	1.91	>0.0001	0.0023	1.81	>0.0001	0.0305	4
neurotrophic factors for neuronal survival, regeneration, and axonal outgrowth	REGULATION_OF_INSULIN_LIKE_GROWTH_FACTOR__IGF__TRANSPORT_AND_UPTAKE_BY_INSULIN_LIKE_GROWTH_FACTOR_BINDING_PROTEINS__IGFBPS__REACTOME	REACT_15428.1	1.96	>0.0001	0.0008	1.08	0.3685	0.6647	4, 5
Notch mediated Schwann cell development	REGULATION_OF_NOTCH_SIGNALING_NCI_NATURE	NCI-Nature PID	1.77	0.0015	0.0189	1.62	0.0114	0.0871	7
Immunocompetence of Schwann cells	NITRIC_OXIDE_STIMULATES_GUANYLATE_CYCLASE_REACTOME	REACT_23862.1	1.96	>0.0001	0.0009	1.27	0.1637	0.3750	2, 3
Schwann cell survival factor mediated signaling	SIGNALING_BY_PDGF_REACTOME	REACT_16888.1	1.70	>0.0001	0.0420	1.56	0.0011	0.1167	1
mesenchymal origin and specialization of Schwann cells	DEVELOPMENTAL BIOLOGY_REACTOME	REACT_111045.1	1.55	>0.0001	0.0884	1.66	>0.0001	0.0614	1
glycosaminoglycan matrix remodeling	MPS_IIIB___SANFILIPPO_SYNDROME_B_REACTOME	REACT_147788.2	1.60	0.0013	0.0656	1.08	0.3369	0.6628	6
neural cell adhesion networks	AXON_GUIDANCE_REACTOME	REACT_18266.1	1.37	0.0061	0.2198	1.70	>0.0001	0.0447	4
proliferation status	CELL_CYCLE__MITOTIC_REACTOME	REACT_152.3	-2.44	>0.0001	>0.0001	0.75	0.9836	0.9587	-
proliferation status	M_PHASE_REACTOME	REACT_910.1	-2.40	>0.0001	>0.0001	-0.86	0.9508	1.0000	-

Supplemental Experimental Procedures

Cell culture

SCC058 foreskin fibroblasts (Millipore) were cultured at 37°C, 5% CO_2 in low serum FibroGro (Millipore). NSC medium consisted of NeuroCult NS-A proliferation medium (StemCell Technologies) supplemented with 1% penicillin/streptomycin, bFGF (20ng/ml), EGF (20ng/ml), BDNF (20ng/ml), Heparin (2µg/ml, Stem Cell Technologies), Dll4 (500ng/ml), Jagged1 (500ng/ml), SHH (500ng/ml, peprotech), Ascorbic Acid (0.2mM, Sigma), FGF8a (100ng/ml), 10% NSC-CM (medium conditioned by ESC-NSCs), and Compound B (2µM, Roche). All growth factors were from R&D systems if not indicated otherwise. To compare effects of other inhibitors, Compound B was replaced by 2µM Dorsomorphin (Tocris), 10µM H89 (Tocris), 10µM Y27632 (Calbiochem), or 10µM GSK650394 (Tocris), respectively.

Neural differentiation medium consisted of N2B27 (1:1 DMEM/F12 and Neurobasal with ß-mercaptoethanol (50µM), B27 supplement without vitamin A (1:50, Invitrogen), and N2 supplement (1:100, Invitrogen)) supplemented with 1% penicillin/streptomycin, BDNF (20ng/ml), GDNF (20ng/ml), Laminin (1µg/ml, Roche), Ascorbic Acid (0.2mM, Sigma) and dibutyryl-cAMP (0.5mM, Sigma).

Adipocyte differentiation medium consisted of DMEM high glucose, 7.5% knockout serum replacement (KOSR, Invitrogen), 0.5% non-essential amino acids, 1% penicillin/streptomycin, 0.1 µM dexamethasone, 10 µg/ml insulin (Sigma) and 0.5 µM rosiglitazone.

Chondrocyte differentiation medium consisted of DMEM high glucose supplemented with 2mM glutamine, 1% pyruvate, 1% penicillin/streptomycin, 1% non-essential amino acids, 10% FCS, and 10ng/ml TGF-β (Peprotech).

To identify compounds that enhance NSC proliferation, NSCs were seeded on POL coated plates at 21000 cells/cm^2 in N2B27. After cell attachment (4h), compounds were added at indicated concentrations. Negative control cells were treated with DMSO. Cells were incubated for four days and subsequently proliferation rate was analyzed by determining the amount of ATP using the CellTiterGlo® kit (Promega) according to the manufacturer's instructions. To analyze the effect of CB on MSCs, ESC-derived MSCs were used (Ahfeldt et al., 2012).

To analyze the effect of CB on NSC differentiation, NSCs were plated on POL coated plates at 60000 cells/cm^2 in N2B27. After cell attachment (4h), CB was added to the cells at indicated concentrations. Cells were incubated for 3 days. Then medium was replaced by fresh N2B27 supplemented with CB. Negative control cells

were treated with DMSO. Cells were incubated for another 4 days and then fixed with 4%PFA and stained for TUJ1. Cells were analysed using a Opera imaging system (Perkin Elmer).

Flow cytometry

Cells were detached and incubated in conditioned medium at 37°C, 5% CO_2 for 2 hours. Cells were stained for 10min at 4°C in MACS running buffer (Miltenyi) containing primary antibodies anti-CD29-PE (BD Bioscience), anti-CD271-APC (Miltenyi), anti-CD146-APC (BD Bioscience) or corresponding isotype controls (BD Bioscience), washed with PBS, and then fixed with 2%PFA for 1hour. Flow cytometry was performed using a BD FACS Canto, and data were analyzed with FlowJo software.

Stainings

Cells were fixed with 4% PFA and then - except for staining of HMMR - permeabilized with 0.1% TritonX. After blocking with 10% donkey serum, cells were stained with primary antibodies overnight. Primary antibodies were anti-TUJ1 (Covance, 1:500), anti-SOX1 (Santacruz, 1:250), anti-NESTIN (Millipore, 1:500), anti-SOX10 (Santacruz, 1:200), anti-SOX2 (Millipore, 1:500), anti-PAX3 (Santacruz, 1:100), anti-SNAI1 (Santacruz, 1:100), anti-FOXD3 (Santacruz, 1:100), anti-PLP (abcam, 1:75), anti-GALC (Millipore, 1:100), anti-KROX20 (Novus Biologicals, 1:100), anti-S100B (abcam, 1:20), anti-MBP (Sigma, 1:100), anti-MAP2 (Sigma, 1:800), anti-GFAP (DAKO, 1:500), anti-HMMR (Novus, 1:250), anti-NF (Covance SMI311, 1:2000 and SMI312, 1:1000), anti-SMA (Dako, 1:100), anti-CD146 (Millipore, 1:500). Subsequently, cells were washed and stained with secondary antibodies conjugated to Alexa 488, 555, and 647 (Molecular Probes). Nuclei were stained with Hoechst (Molecular Probes). Cells were imaged using a Zeiss inverted microscope. Images were analyzed using ImageJ software. Quantifications of PLP and MAP2 stainings were performed using an Operetta imaging system and the Harmony image analysis software (PerkinElmer).

For Oil Red O staining, cells were fixed with 4% PFA, washed with PBS and incubated in Oil Red O staining solution (0.18% Oil Red O in 60% isopropanol) for one hour. Subsequently, cells were washed 3-5 times with PBS and analyzed.

For Alcian Blue staining, cell pellet was fixed with 4% PFA, washed 3 times with PBS and incubated in Alcian Blue staining solution (0.01% Alcian Blue 8 GX in 60% ethanol, 40% acetic acid) overnight. Pellet was destained 3 times for 20min with Destaining solution (60% ethanol, 40% acetic acid), transferred to PBS and analyzed.

Electrophysiology

Pipettes with a tip resistance of 3–4 MΩ were made from borosilicate capillaries (Harvard Apparatus Ltd) with a DMZ-Universal micropipette puller (Zeitz Instrumente) and filled with a solution containing (in mM): Potassium-D-gluconate 135.0, KCl 20.0, $MgCl_2$ 2.0, HEPES 10.0, EGTA 0.1, Na_2-ATP 2.0, Na_3-GTP 0.3 (pH 7.3 with KOH, osmolarity 300 mmol/kg). Coverslips with cells were placed in a chamber mounted on the stage of an inverted microscope (Nikon TE300) and constantly perfused with an extracellular solution containing (in mM): NaCl 149.0, KCl 3.25, $CaCl_2$ 2.0, $MgCl_2$ 2.0, HEPES 10.0, D(+)-glucose monohydrate 11.0 (pH 7.35 with NaOH, osmolarity 315 mmol/kg). Membrane currents were recorded using a MultiClamp 700B amplifier connected to a Digidata 1322A digitizer (Molecular Devices). Data acquisition, storage, and analysis were performed with Clampex and ClampFit (Molecular Devices). Series resistance was not compensated but leak substraction was sometimes performed. Data were sampled at 50 KHz. Resting membrane potential was measured in current-clamp immediately after having reached the whole cell configuration. Action potentials were evoked under current-clamp by applying variable pulses of current (500-1000pA) to the neurons. The presence of voltage-gated Na^+ - and K^+ - channels was assessed in the voltage-clamp configuration.

Genome-wide gene expression analysis

For total RNA extraction, cells were homogenized in tubes prefilled with 1.4 mm ceramic beads and QIAzol lysis reagent using a FastPrep-24 instrument (MP Biomedicals) and the Qiagen miRNeasy Mini Kit with DNase treatment (Qiagen). RNA quality assessment and quantification was performed using microfluidic chip analysis on an Agilent 2100 bioanalyzer (Agilent Technologies). On a Biomek FXp workstation (Beckman Coulter), 10ng of total RNA was reverse transcribed using the NuGen Ovation Pico WTA Systems V2, followed by fragmentation, and 3'-biotin-labeling with the NuGen Encore Biotin module (NuGEN Technologies). 4.4µg fragmented cDNA were hybridized for 16 h at 45ºC and 65 rpm on an Affymetrix HG-U133_plus_2 microarray followed by washing, staining, and scanning on a GeneChip Fluidics 450 station and a GeneChip Scanner 3000 (Affymetrix). Affymetrix probe intensities were subjected to robust multi-array analysis (RMA), background correction with quantile normalization, and a median polish probeset summarization as implemented in the Partek Genomics Suite 6.6 software (Partek). Gene names for the probesets were identified using Partek and NetAffyx (Affymetrix). Gene Ontology (GO) term analysis of gene lists was performed using DAVID Bioinformatics Resource (http://david.abcc.ncifcrf.gov/). Gene Set Enrichment Analysis was applied to the data

on the basis of the BROAD Institute algorithm (http://www.broadinstitute.org/gsea). Log_2 Fold Changes were used to rank the genes and to determine the enrichment of genes in gene sets derived from the union of the Reactome signaling pathway database (http://www.reactome.org/) and the NCI-Nature Pathway Interaction Database (http://pid.nci.nih.gov/). For all GSEA analyses 1000 phenotype permutations were performed to assess the significance of the enrichment. GSEA results passing significance thresholds (p-value < 0.005, False Discovery Rate q-value < 0.1) were visualized as a network of gene sets (nodes) related by overlapping genes (edges) using the Cytoscape plug-in enrichment map (http://www.baderlab.org/). Gene expression heat maps were generated using the R software for statistical computing and graphics (http://www.r-project.org/).

Supplemental References

Ahfeldt, T., Schinzel, R.T., Lee, Y.K., Hendrickson, D., Kaplan, A., Lum, D.H., Camahort, R., Xia, F., Shay, J., Rhee, E.P., *et al.* (2012). Programming human pluripotent stem cells into white and brown adipocytes. Nat Cell Biol *14*, 209-219.

Ambasudhan, R., Talantova, M., Coleman, R., Yuan, X., Zhu, S., Lipton, S.A., and Ding, S. (2011). Direct reprogramming of adult human fibroblasts to functional neurons under defined conditions. Cell Stem Cell *9*, 113-118.

Bhatheja, K., and Field, J. (2006). Schwann cells: origins and role in axonal maintenance and regeneration. Int J Biochem Cell Biol *38*, 1995-1999.

Fu, J.D., Stone, N.R., Liu, L., Spencer, C.I., Qian, L., Hayashi, Y., Delgado-Olguin, P., Ding, S., Bruneau, B.G., and Srivastava, D. (2013). Direct Reprogramming of Human Fibroblasts toward a Cardiomyocyte-like State. Stem Cell Reports *1*, 235-247.

Higginson, J.R., Thompson, S.M., Santos-Silva, A., Guimond, S.E., Turnbull, J.E., and Barnett, S.C. (2012). Differential sulfation remodelling of heparan sulfate by extracellular 6-O-sulfatases regulates fibroblast growth factor-induced boundary formation by glial cells: implications for glial cell transplantation. J Neurosci *32*, 15902-15912.

Meyer zu Horste, G., Hu, W., Hartung, H.P., Lehmann, H.C., and Kieseier, B.C. (2008). The immunocompetence of Schwann cells. Muscle Nerve *37*, 3-13.

Nam, Y.J., Song, K., Luo, X., Daniel, E., Lambeth, K., West, K., Hill, J.A., DiMaio, J.M., Baker, L.A., Bassel-Duby, R., *et al.* (2013). Reprogramming of human fibroblasts toward a cardiac fate. Proc Natl Acad Sci U S A *110*, 5588-5593.

Outani, H., Okada, M., Yamashita, A., Nakagawa, K., Yoshikawa, H., and Tsumaki, N. (2013). Direct induction of chondrogenic cells from human dermal fibroblast culture by defined factors. PLoS One *8*, e77365.

Pang, Z.P., Yang, N., Vierbuchen, T., Ostermeier, A., Fuentes, D.R., Yang, T.Q., Citri, A., Sebastiano, V., Marro, S., Sudhof, T.C., *et al.* (2011). Induction of human neuronal cells by defined transcription factors. Nature *476*, 220-223.

Raivich, G., and Makwana, M. (2007). The making of successful axonal regeneration: genes, molecules and signal transduction pathways. Brain Res Rev *53*, 287-311.

Woodhoo, A., Alonso, M.B., Droggiti, A., Turmaine, M., D'Antonio, M., Parkinson, D.B., Wilton, D.K., Al-Shawi, R., Simons, P., Shen, J., *et al.* (2009). Notch controls embryonic Schwann cell differentiation, postnatal myelination and adult plasticity. Nat Neurosci *12*, 839-847.

Woodhoo, A., and Sommer, L. (2008). Development of the Schwann cell lineage: from the neural crest to the myelinated nerve. Glia *56*, 1481-1490.

Ydens, E., Lornet, G., Smits, V., Goethals, S., Timmerman, V., and Janssens, S. (2013). The neuroinflammatory role of Schwann cells in disease. Neurobiol Dis *55*, 95-103.

Zhang, K., Liu, G.H., Yi, F., Montserrat, N., Hishida, T., Esteban, C.R., and Izpisua Belmonte, J.C. (2014). Direct conversion of human fibroblasts into retinal pigment epithelium-like cells by defined factors. Protein Cell *5*, 48-58.